Environmental Pollution 300 (2022) 118964

Contents lists available at ScienceDirect

Environmental Pollution

journal homepage: www.elsevier.com/locate/envpol

Visualization and (Semi-)quantification of submicrometer plastics through scanning electron microscopy and time-of-flight secondary ion mass spectrometry☆

Shih-Hsuan Chou [a,b], Yung-Kun Chuang [b], Chi-Ming Lee [c], Yu-Shan Chang [b], Ya-Jhu Jhang [d], Ching-Wen Yeh [b], Tai-Sing Wu [e], Chun-Yu Chuang [a], I-Lun Hsiao [b,f,*]

[a] Department of Biomedical Engineering and Environmental Sciences, National Tsing Hua University, Hsinchu, 30013, Taiwan
[b] Master Program in Food Safety, College of Nutrition, Taipei Medical University, Taipei, 10031, Taiwan
[c] Core Facility Center, Office of Research and Development, Taipei Medical University, Taipei, 10031, Taiwan
[d] Institute of Analytical and Environmental Sciences, National Tsing Hua University, Hsinchu, 30013, Taiwan
[e] National Synchrotron Radiation Research Center (NSRRC), Hsinchu, 30013, Taiwan
[f] School of Food Safety, College of Nutrition, Taipei Medical University, Taipei, 11031, Taiwan

ARTICLE INFO

Keywords:
Nanoplastics
Tea bags
Coffee-ring effect
ToF-SIMS
Nanoparticle tracking analysis

ABSTRACT

Increasing numbers of studies have demonstrated the existence of nanoplastics (1–999 nm) in the environment and commercial products, but the current technologies for detecting and quantifying nanoplastics are still developing. Herein, we present a combination of two techniques, e.g., scanning electron microscopy (SEM) and time-of-flight secondary ion mass spectrometry (ToF-SIMS), to analyze submicron-sized plastics. A drop-casting of a 20-nL particle suspension on a Piranha solution-cleaned silicon wafer with dry ice incubation and subsequent freeze-drying was used to suppress the coffee-ring effect. SEM images were used to quantify particles, and this technique is applicable for 0.195–1.04-μm polystyrene (PS), 0.311-μm polyethylene terephthalate (PET), and 0.344-μm polyethylene (PE) at a minimum concentration of 2.49×10^9 particles/mL. ToF-SIMS could not quantify the particle number, while it could semi-quantitatively estimate number ratios of submicron PE, PET, polyvinyl chloride (PVC), and PS particles in the mixture. Analysis of submicron plastics released from three hot water-steeped teabags (respectively made of PET/PE, polylactic acid (PLA), and PET) was revisited. The SEM-derived sizes and particle numbers were comparable to those measured by a nanoparticle tracking analysis (NTA) regardless of whether or not the hydro-soluble oligomers were removed. ToF-SIMS further confirmed the number ratios of different particles from a PET/PE composite teabag leachate. This method shows potential for application in analyzing more-complex plastic particles released from food contact materials.

1. Introduction

Increasing numbers of nanoplastics-related publications have been released since 2016, and recently nanoscientists consider that these particles should be regarded as a significant source of global plastic pollution and a distinct issue from microplastics and engineered nanoparticles (Gigault et al., 2021; Mitrano et al., 2021). Currently, due to the lack of universal and robust analytical methods, there are few data demonstrating the presence of nanoplastics (1–999 nm) in the environment, manufacturing, and products, for example, in seawater of the North Atlantic subtropical gyre (TerHalle et al., 2017), snow pit and surface snow in the Austrian Alps (Materić et al., 2020), recycled commodity polyvinyl chloride (PVC) powder (Zhang et al., 2020), facial scrubs (Hernandez et al., 2017), hot water-treated tea bags (Hernandez et al., 2019), and laser printers (Fang et al., 2021).

The same as with microplastics, the particle size, morphology, amount, and chemical composition are four important characteristics of nanoplastics with which scientists are concerned. Mass spectrometry (MS)-based methods, for example, thermo desorption-proton transfer reaction (TD-PTR)-MS (Materić et al., 2020), pyrolysis gas chromatography (Py-GC)-MS (Zhou et al., 2019), thermal extraction and desorption (TED)-GC-MS (Dümichen et al., 2017), and thermal pretreatment

☆ This paper has been recommended for acceptance by Eddy Y. Zeng.

* Corresponding author. School of Food Safety, College of Nutrition, Taipei Medical University, Taipei, 11031, Taiwan.
E-mail address: ilunhsiao@tmu.edu.tw (I.-L. Hsiao).

https://doi.org/10.1016/j.envpol.2022.118964
Received 5 November 2021; Received in revised form 3 February 2022; Accepted 4 February 2022
Available online 5 February 2022

following matrix-assisted laser desorption/ionization time-of-flight (MALDI-ToF)-MS can provide quantitative information on different nanoplastics in mass units with limits of detection of 10–100 ng (Lin et al., 2020). However, separation of micro- and nanosized particles in advance is required, and combinations of other characterization techniques such as electron microscopy and asymmetric flow field flow fractionation (AF4) coupled with multiangle light scattering (MALS) are required to offer size and morphology information (Mintenig et al., 2018).

On the basis of Raman spectroscopic technologies, Raman tweezers (RTs) (Gillibert et al., 2019), centrifugal field-flow fractionation (CF3) coupled with MALS and RTs (Schwaferts et al., 2020), image resolution-improved confocal Raman imaging (Fang et al., 2020), and correlative Raman imaging and scanning electron (RISE) microscopy (Zhang et al., 2020) are able to identify a single plastic particle with a limit of detection of size ranging 30–360 nm. Size (primary or secondary) and morphology data are also available. The former two methods, used to analyze liquid dispersions, need a minimum concentration of 10^9 particles/L, while a quantification protocol for the latter two dry-based methods is still lacking. Nile red plastic staining with subsequent single-particle tracking can detect 2×10^6 particles/mL and a minimum size of 45-nm polystyrene (PS) particles (Molenaar et al., 2021). The staining capability of different types of plastic and selectivity to plastic and non-plastic particles still need to be proven.

Scanning electron microscopy (SEM) can produce nanoscale resolution imaging of nano/micro-sized materials through a high-energy electron beam. In nanoplastic-related studies, it was used to obtain the surface morphology of recycled commodity PVC powder (Zhang et al., 2020) and nanoparticles in polyethylene (PE)-containing commercial scrubs (Hernandez et al., 2017), and even to quantify the micro/nanoplastics released from hot water-treated tea bags (Hernandez et al., 2019). However, a method is needed to identify particle compositions. Time-of-flight secondary ion MS (ToF-SIMS) can obtain submicrometer-resolution mass imaging by utilizing a primary ion gun, which has a beam spot size of nano-to submicron-scale, as a probe. Sputtered fragment ions of 0.1–2 nm of a solid surface can be identified by a ToF mass analyzer with a mass resolution of ~9000. This technique has been used to identify degraded PE pellets in a mixture of Ottawa sand after 14 days of sea surf simulation, and a size down to 1 μm could be detected (Jungnickel et al., 2016). We suspect that it has potential to identify submicrometer plastics as well. Furthermore, to develop a particle number quantification method for the abovementioned two techniques, a reliable drop-casting method which eliminates heterogeneity of the particle distribution after drying of liquid droplets needs to be developed.

The objective of this study was to develop a new strategy for quantifying plastic particles at the submicron-scale. A dry ice-incubated super-hydrophilic silicon wafer with a subsequent freeze-drying process was selected for the drop-casting method. Applicable working conditions were tested on various sizes (0.99, 0.195, 0.305, and 1.040 μm) and concentrations of PS particles by SEM. The differentiation capability and semi-quantification of the mixtures of submicron plastics (including self-prepared PE, polyethylene terephthalate (PET), PVC, and commercial PS submicron particles) using ToF-SIMS were validated. Finally, the techniques were applied to characterize submicron-sized plastics released from hot water-treated tea bags, in which the size and number concentration were compared to those determined using a nanoparticle tracking analysis (NTA).

2. Material and methods

2.1. Chemicals, commercial submicron plastics, and commercial teabags

PVC (with a weight average molecular weight (M_w) of ~43,000 and a number average molecular weight (M_n) of ~22,000), PE (with an M_w of ~4000 and an M_n of ~1700), sulfuric acid, acetone, ethanol, hydrogen peroxide, and 1,1,1,3,3,3-hexafluoro-2-propanol (HFIP) (>99%) were purchased from Sigma-Aldrich (Steinheim, Germany). Tween 80 and Span 80 were purchased from Xilong Scientific (Guangdong, China). Tetrahydrofuran (THF) was purchased from Merck Millipore (Darmstadt, Germany). Trifluoroacetic acid (TFA) was purchased from Fluorochem (Derbyshire, UK). Toluene and methanol were purchased from J.T. Baker (Phillipsburg, NJ, USA). PET (<300 μm) was purchased from Goodfellow (Coraopolis, PA, USA). Non-functionalized PS microspheres (0.099, 0.195, 0.305, and 1.040 μm in diameter) were purchased from Bangs Laboratories (Fishers, IN, USA). Trifluoroethanol (TFE) was purchased from Alfa Aesar (Ward Hill, MA, USA). Three different types of commercial plastic teabags were bought from grocery stores in Taipei, Taiwan.

2.2. Visualization and quantitative analysis of submicron PS using SEM

A linear relationship of an SEM-based quantitative method was determined using various sizes of PS standards (0.99, 0.195, 0.305, and 1.040 μm) and different particle number concentrations. Particle number concentrations of PS aqueous stock solutions were first determined by an NTA (NanoSight NS300, Malvern, Worcestershire, UK). Because submicron-sized plastics in the environment may contain PE or PP with a density of less than water (1 g/cm^3) and may not be well suspended, we used a methanol/water solution (methanol: water = 20:12.5, v/v) instead of an aqueous solution to suspend and dilute all particle suspensions.

To obtain a super-hydrophilic silicon wafer, diced silicon wafers were cleaned by treating them in Piranha solution (sulfuric acid: 30% hydrogen peroxide = 3:1, v/v) for 10 min. Then, the silicon wafers were washed with deionized water and dried at 85 °C for later use.

A freeze-drying method was selected to suppress the coffee-ring effect during drop-casting. First, a super hydrophilic silicon wafer was placed in a Petri dish and put on a piece of dry ice until the surface of the wafer was frozen (Fig. 1). A 20-nL suspension was dripped onto the frozen silicon wafer via a 0.5-μL microsyringe (Hamilton, Reno, NV, USA). The droplet immediately turned into ice on the wafer. Then, the wafer-containing Petri dish was placed into a −30 °C pre-incubated freeze-drying flask and incubated for 30 min. Finally, the flask was immediately loaded into a freeze-dryer and dried for 30 min (UNISS, New Taipei City, Taiwan).

For each droplet, a full-area image and 10 randomly selected partial-area images were obtained using the secondary electron mode of SEM (Hitachi SU3500, Tokyo, Japan) without sputter coating. Then the full droplet area and partial areas (observed at 3000 × or 10^4 ×) of images were analyzed by ImageJ software (LOCI, Madison, WI, USA). The number of particles was manually counted.

Equation (1) was used to calculate the total particle number in the entire area:

$$SEM\text{-derived particle number} = \frac{Full\ droplet\ area}{Partial\ magnified\ area} \times Average\ particle\ number\ in\ 10\ images. \quad (1)$$

The particle number concentration was calculated by equation (2):

$$Particle\ number\ concentration\ (\#/mL) = \frac{SEM\text{-derived particle number}}{20 \times 10^{-6}(droplet\ volume)} \quad (2)$$

Due to the error of the particle number concentration provided by the PS manufacturer and NTA measurement being within ±10%, the former value was used as a reference and was compared to the SEM-derived number concentration to obtain the relative error (%).

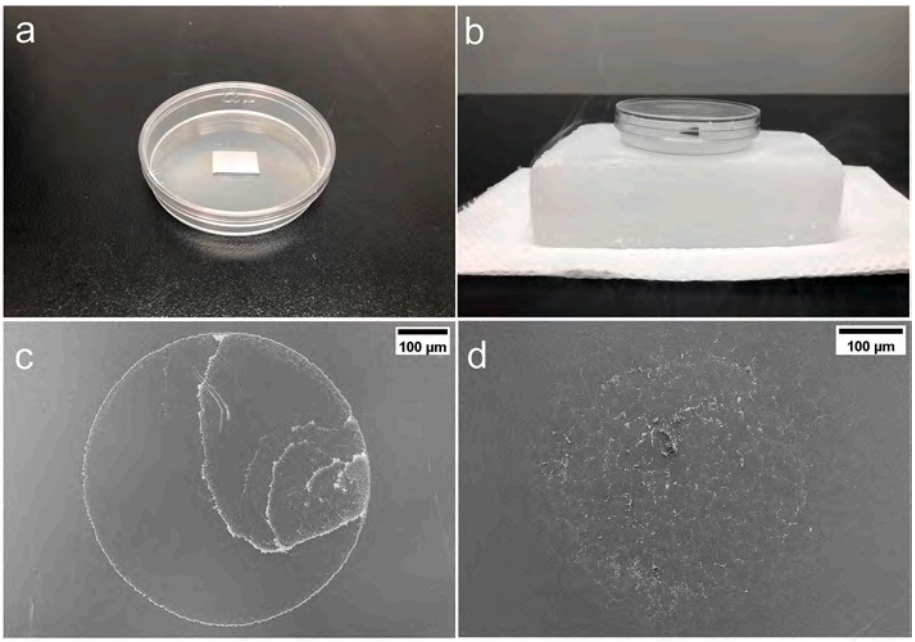

Fig. 1. Suppression of the coffee-ring effect in a dry-ice-incubated submicron polystyrene (PS) droplet with freeze-dried casting. A submicron PS (20 nL, 0.305 μm) suspension was dropped onto a silicon wafer without (a) and with underlying dry-ice treatment (b) and their corresponding SEM images (c and d). (For interpretation of the references to colour in this figure legend, the reader is referred to the Web version of this article.)

2.3. Validation of the (semi)-quantitative analysis by ToF-SIMS

To examine whether ToF-SIMS could quantify different types of submicron plastics, a mixed suspension with a known number concentration (4.94×10^9 particles/mL) containing as-prepared submicron PE, PET, PVC (see Supplemental Information (SI) for details of the method), and 0.305-μm PS particles with a number ratio of 0.94:1:0.9:1 was prepared in a methanol-water solvent. Number concentrations of stock submicron PVC and PS particles were determined by the NTA, and the others were evaluated by SEM. Then, a 20-nL suspension was used to prepare a sample by the above-described process. The SEM-derived particle concentration was compared to known concentrations of particle mixtures to ensure successful sample preparation. The ToF-SIMS analysis (ULVAC-PHI TRIFT IV, Kanagawa, Japan) was carried out using 30 keV of a Bi_3^{++} primary ion beam at a dose density of 4.9×10^{12} ions/cm^2, and positively charged secondary ions were collected. The Bi_3^{++} beam was selected in this study because it provides higher spatial resolution than the Bi^+ or Bi_3^+ primary ion for analyzing inorganic and organic materials due to its higher kinetic energy (Holzlechner et al., 2013; Shishido et al., 2016). The scanning area, collection time, and imaging resolution were 200 × 200 μm^2, 1 h, and 1024 × 1024 pixels, respectively.

Representative m/z values were selected, and ion images were overlaid as the image of a specific polymer using WinCadence software. PE was differentiated by m/z values of 69.07 ($C_5H_9^+$), 111.01 ($C_8H_{15}^+$), and 141.04 ($C_{10}H_{21}^+$), PET by m/z values of 104.03 ($C_7H_4O^+$), 105.04 ($C_7H_5O^+$), and 165.06 ($C_8H_5O_4^+$), PVC by an m/z of 61.99 ($C_2H_3Cl^+$), and PS was differentiated by an m/z ratio of 91.05 ($C_7H_7^+$). The choice of peaks for all plastics depended upon known characteristic ions from each standard spectrum which did not overlap with each other (Abmayr, 2006; Kern et al., 2019). To further examine the capability of particle-by-particle identification using ToF-SIMS, a silicon wafer with only 0.305-μm PS particles was prepared, and then ToF-SIMS and SEM images were captured at an approximate location. The number of detected pixels contained in each image was calculated by ImageJ software to estimate the numbers of plastic particles and their ratios. Brightness and sharpness of the ion images were adjusted to make them more visible for the presentation.

2.4. Analysis of submicron plastics released after hot-water treatment of teabags

2.4.1. Teabags

Three types of teabags were purchased from grocery stores in Taipei City, Taiwan. One teabag did not contain tea leaves, while the other two did. The chemical composition of the teabags was confirmed using attenuated total reflection-Fourier transform infrared spectroscopy (ATR-FTIR, Nicolet-6700, ThermoFisher Scientific, Waltham, MA, USA) with a deuterated triglycine sulphate (DTGS) detector. Three positions were randomly selected when measuring each teabag.

2.4.2. Hot-water steeping

All tea leaves in the teabags were removed with scissors. Deionized water was filtered through a 100-kDa membrane with a stirred cell system (UHP–43K, Advantec, Tokyo, Japan) to remove most particulates. Then, the filtered water was heated to 95 °C. Three identical teabags were placed into a 50-mL polypropylene (PP) centrifuge tube. Hot water (15 mL) at 95 °C was added, and the teabags were steeped for 8 min at room temperature. During the process, the teabags were completely submerged under the water. Then, the centrifuge tube was vortexed. Water remaining in the teabags was squeezed out with stainless steel tweezers. Fresh water (5 mL) was used to wash the teabags, and the final volume of the leachate was 20 mL. The above-described experimental procedures were performed in a clean centrifuge tube without teabags as a blank.

The hydrodynamic diameter and number concentration of plastic particles in the leachate were directly analyzed by an NTA (488-nm laser). For each measurement, triplicate videos were randomly captured and collected for 60 s. The primary size, number concentration, and morphology of the plastic particles were obtained by an SEM quantitative method. Methanol (800 μL) and 500 μL of teabag leachate were mixed. Then, the suspension was either directly dripped onto a silicon wafer or concentrated by centrifugation (20,000×*g*, 20 min) before dripping to achieve the required concentration. Finally, ion images were created by ToF-SIMS. The scanning area, collection time, and imaging resolution were 200 × 200 μm^2, 1 h, and 1024 × 1024 pixels, respectively.

2.4.3. Oligomer removal from the leachate

To remove possible oligomers existing in the three teabag leachates, 10 mL of teabag leachate was added to a centrifugal concentrator with a 100-kDa membrane (Vivaspin® Turbo 15, Sartorius AG, Göttingen, Germany) and centrifuged at 2000×*g* for 17 min. Then, the bottom solution (with oligomers only) was collected for subsequent experiments. Deionized water (10 mL) was added to the upper concentrate tube, particles on the membrane were re-suspended using ultrasonic probe treatment (30 W, 2 min) (Q125, Qsonica, Newtown, CT, USA), and the suspension was also collected. The number concentration and size detected by the NTA or derived via SEM were determined.

To demonstrate the removal of oligomers in three teabag leachates, the upper suspensions (supposedly containing only particles) were filtered through a 100-kDa membrane with a stirred cell system to remove particles. Then, 5 mL of the upper suspension leachate and bottom solution was concentrated to 0.5 mL by freeze-dying. A 0.5-mL mixture of HFIP/THE/ethanol (2:2:4, v/v/v) was added to a final volume of 1 mL. Finally, the 1-mL sample was filtered using a 0.22-μm PTEF filter before LC-MS qualitative detection for PET or polylactic acid (PLA) oligomers. A method blank was performed using deionized water only, and it was separated into upper and bottom blank samples as well. Conditions for the LC-MS operation are described in SI.

3. Results and discussion

3.1. Suppression of the coffee-ring effect

When a non-volatile nanoparticle-containing droplet is dropped onto a solid surface such as a silicon wafer, the dominant outward capillary flow and weak inward Marangoni flow of the volatile solvent drive the solutes to the contact line of the droplet, which leads to a ring-like deposit, and the so-called "coffee-ring effect". One strategy to suppress this phenomenon is to weaken the outward capillary flow (Anyfantakis et al., 2015; He et al., 2019; Sun et al., 2015). Herein, we developed dry-ice incubation followed by freeze-drying as a solution.

Silicon wafers incubated without and with dry ice when the 0.305-μm PS was dripped onto the surface and their corresponding SEM images after freeze-drying are shown in Fig. 1. The former without dry ice had an obvious "coffee ring" around the edge of droplet, while the latter, in contrast, was relatively uniform. Droplets were dripped onto a solid substrate under dry-ice incubation (ca. −76 °C), so that the droplets immediately froze, which prevented capillary flow from occurring both before and following freeze-drying. It was noted that if the temperature of the solid substrate was not low enough (<-5 °C), the particles still moved to the edge due to the formation of a quasi-liquid layer (He et al., 2019).

To clarify the necessity of cleaning the silicon wafers with Piranha solution in the protocol, 0.305-μm PS was also dripped onto a wafer

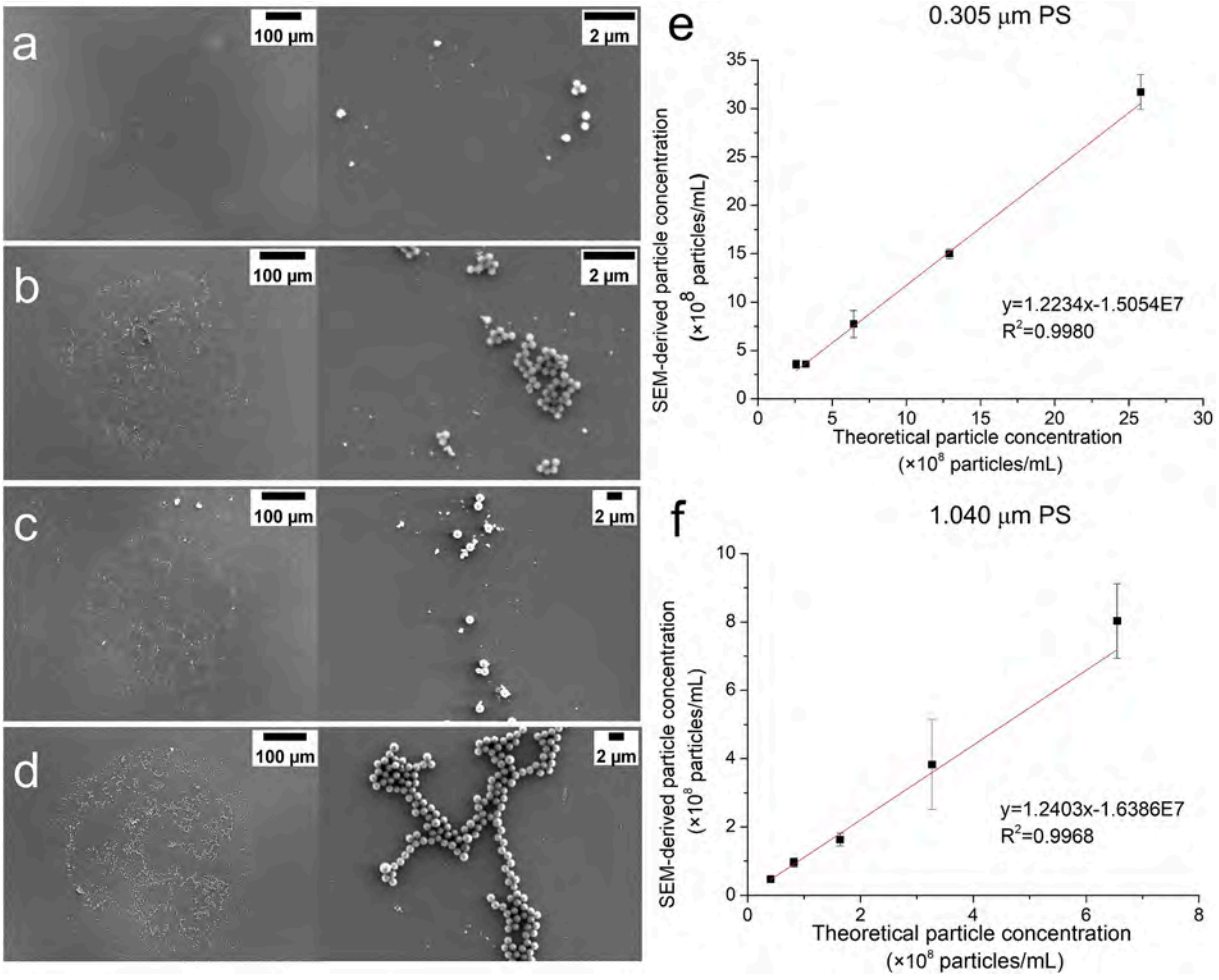

Fig. 2. Linear relations of submicron polystyrene (PS) using an SEM quantification method. SEM images of a full droplet (left) and a partially magnified (right) area at (a) the lowest and (b) the highest number concentrations of 0.305-μm PS. A full droplet (left) and partially magnified droplet at (c) the lowest and (d) highest number concentrations of 1.040-μm PS are shown. The linear relationship of (e) 0.305 and (f) 1.040 μm between theoretical and SEM-derived particle concentrations ($n = 3$). Both R^2 values reached >0.995.

without the cleaning step. Even though using dry-ice incubation with subsequent freeze-drying, the PS particles aggregated and were centralized without Piranha treatment (Fig. S1). The lower contact angle (<90°) between the droplet and hydrophilic silicon substrate verified that the substrate had high surface energy, which explains the even stacking of particles on the Piranha-treated silicon wafer. In contrast, the untreated silicon wafer had a higher contact angle (>90°), which explains the more-numerous, stacked PS agglomerates (Franssila, 2010).

3.2. Quantification of submicron plastics by SEM

Fig. 2a–d shows the representative entire and partial areas of SEM images for 0.305- and 1.040-μm PS at the lowest and highest concentrations. Linear relations of the SEM quantitative method are shown in Fig. 2. R^2 of the calibration curve for 0.305-μm PS at 2.58×10^8–2.58×10^9 particles/mL was 0.9980, and it was 0.9968 for 1.040-μm PS at 4.10×10^7–6.55×10^8 particles/mL. The relative errors were 12%~38% and −1%~23% for 0.305- and 1.040-μm PS, respectively (Table S1). However, large, irregularly shaped aggregates formed and could not be quantified when the concentrations of PS were 2.15×10^8 and 2.05×10^7 particles/mL for 0.305- and 1.040-μm PS, respectively (Fig. S2). PS at 0.195 μm could be quantified at 2.49×10^9 particles/mL with a relative error of −6%±3%, while aggregates formed at 6.25×10^8 particles/mL (Fig. S3). Unfortunately, 0.099-μm PS formed aggregates at 3.83×10^9–3.83×10^{10} particles/mL (Fig. S2). Thus, as the number concentration exceeded 2.49×10^9 particles/mL, 0.195- to 1.040-μm PS could effectively be quantified. It seems that the smaller the PS diameter was, the higher the concentration that was required for analysis. In the freeze-drying process, the heterogeneous freezing of a droplet is induced by the PS particles. With smaller and a lower concentration of PS particles, the freezing speed was relatively lower. PS particles, as impurities, were more likely to be concentrated in grain boundaries of ice crystals and cause squeezing deformations. On the contrary, with a higher freezing speed, the PS particles were more likely to be incorporated into ice matrixes.

3.3. Detection of submicron plastics using ToF-SIMS

3.3.1. Effects of aged micro/submicron plastics on ToF-SIMS

To ensure that ToF-SIMS could identify the plastic type regardless of whether they were aged or not, PE microplastics (<74 μm) were exposed to UV light for 0–15 days, and both positive and negative ions of ToF-SIMS were collected for microplastics (for details of the method, see SI; Fig. S4). The main characteristic m/z peaks of PE significantly changed to oxidation peaks in the negative ion model after 2 days of irradiation. However, the main characteristic peaks in the positive ion model did not change at any time points (Fig. S5). Therefore, in this study, we collected positive ions for subsequent experiments.

3.3.2. Characterization of as-prepared and commercial submicron-plastics

PVC, PET, and PE submicron-particles were prepared to validate semiquantitative detection using ToF-SIMS. TEM images showed that PVC nanoparticles had a spherical shape and were 238 ± 41 nm in diameter. PET and PE nanoparticles had irregular shapes and were 311 ± 109 and 344 ± 202 nm in diameter, respectively (Fig. 3). DLS measurements showed that PVC and PET had hydrodynamic diameters of 293 ± 41 and 932 ± 61 nm with respective values of the polydispersity index (PdI) of 0.13 and 0.44 (Fig. S6). Commercial 0.305-μm PS had a spherical shape, and particles were 316 ± 18 nm in diameter according to TEM. PS had a hydrodynamic diameter of 591 ± 13 nm with a PdI of 0.15 as measured by DLS (Fig. S6). The NTA showed that the number concentrations of submicron PVC and PS were $2.41 \pm 0.61 \times 10^{10}$ (230 ± 3 nm) and $6.90 \pm 1.23 \times 10^{12}$ particles/mL (282 ± 6 nm), respectively. Due to PET and PE submicron particles not being stable or well suspended in water, the number concentration was measured by SEM developed in this study rather than by the NTA. SEM images showed that the homogeneity of particles of both PET and PE on the silicon wafers was similar to that of PS, indicating that the method was also applicable to different plastic types (Fig. 3). Number concentrations of submicron PET and PE were $5.15 \pm 1.53 \times 10^9$ and $4.18 \pm 0.92 \times 10^9$ particles/mL, respectively.

3.3.3. Validation of the semiquantitative analysis

A mixture of self-synthesized, 0.344-μm PE, 0.311-μm PET, 0.238-μm PVC, and commercial 0.305-μm PS with a known particle number ratio

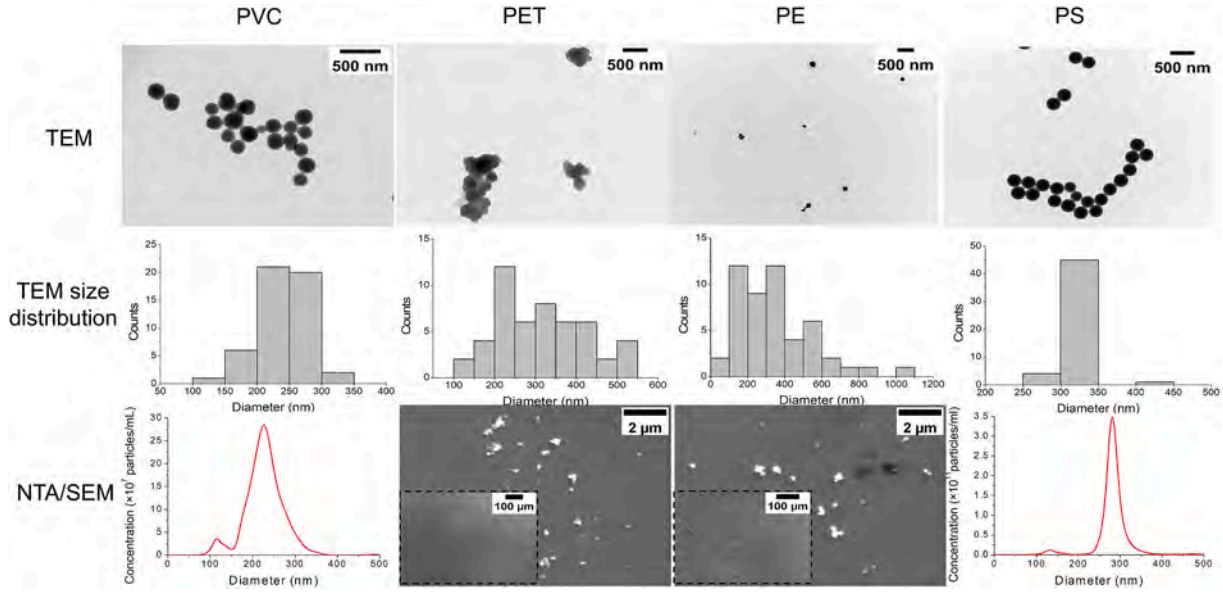

Fig. 3. Primary size, morphology, and number concentration of self-synthesized and commercial polystyrene (PS) submicron plastics. Data on the former two were acquired by TEM, and the latter was derived via a nanoparticle tracking analysis (NTA) or SEM quantification method. Fifty particles were analyzed to derive the TEM size. A representative SEM image of full and partially magnified droplets used for quantification are shown for polyethylene terephthalate (PET) and polyethylene (PE) submicron plastics.

was prepared. Fig. 4 shows representative SEM images of the mixed particles in full-droplet and partial-droplet areas, and the number concentration was $6.15 \times 10^9 \pm 3.89 \times 10^9$ particles/mL. Compared to the theoretical concentration (4.94×10^9 particles/mL), the relative error was 24%, indicating that the SEM-based quantification method also worked relatively well for a mixture of different submicron plastics. Fig. 4 shows ToF-SIMS total ions, spectrum, and specific ion images which represented different plastics. Distribution patterns of the four different plastics (i.e., PE, PET, PVC, and PS) were similar due to their being well-mixed in the methanol/water solution. However, the planar images were slightly distorted because of the 45° incidence angle of the primary ion beam (Rangarajan and Tyler, 2006). Due to similar sizes among the four plastics, we estimated particle numbers using detected pixel numbers in the images with a pixel size of 195 nm. Respective pixel numbers of PE, PET, PVC, and PS were 1658, 1959, 1784, and 1902, which corresponded to 8812, 10,412, 9482, and 10,109 in the entire droplet area (212,596 μm^2). The numbers were underestimated compared to the theoretical particle numbers (24,200, 25,800, 23,000, and 25,800, respectively), suggesting that submicron plastic particles were likely not able to be quantified by ToF-SIMS. Fig. S7 shows SEM and ToF-SIMS images of 0.305-μm PS in the approximate partial droplet area. It was clearly observed that ToF-SIMS failed to identify all particles shown in the SEM image. By analyzing detected pixel numbers, particle numbers were again underestimated (8052 for detected and 25,800 for theoretical particles). Surprisingly, the ToF-SIMS detected signal showed no particles in SEM. The underestimation might be explained by insufficient lateral resolution, influence of ionization probability by the matrix, and/or an uneven particle arrangement that caused variant top atomic layers between particles (Bennet et al., 2020). The undesired signal might have resulted from residual PS oligomers in the commercial product. Nevertheless, the number ratios of the four submicron plastics were 0.85:1:0.91:0.97 for PE: PET: PVC: PS and 0.95 ± 0.1:1 $\pm$ 0:1.17 $\pm$ 0.26:0.88 $\pm$ 0.09 for a combination of another independent replication ($n = 2$), which were similar to the theoretical ratio of the different plastics (0.94:1:0.9:1). This suggests that ToF-SIMS can be used as a semiquantitative method to evaluate ratios of submicron plastic numbers.

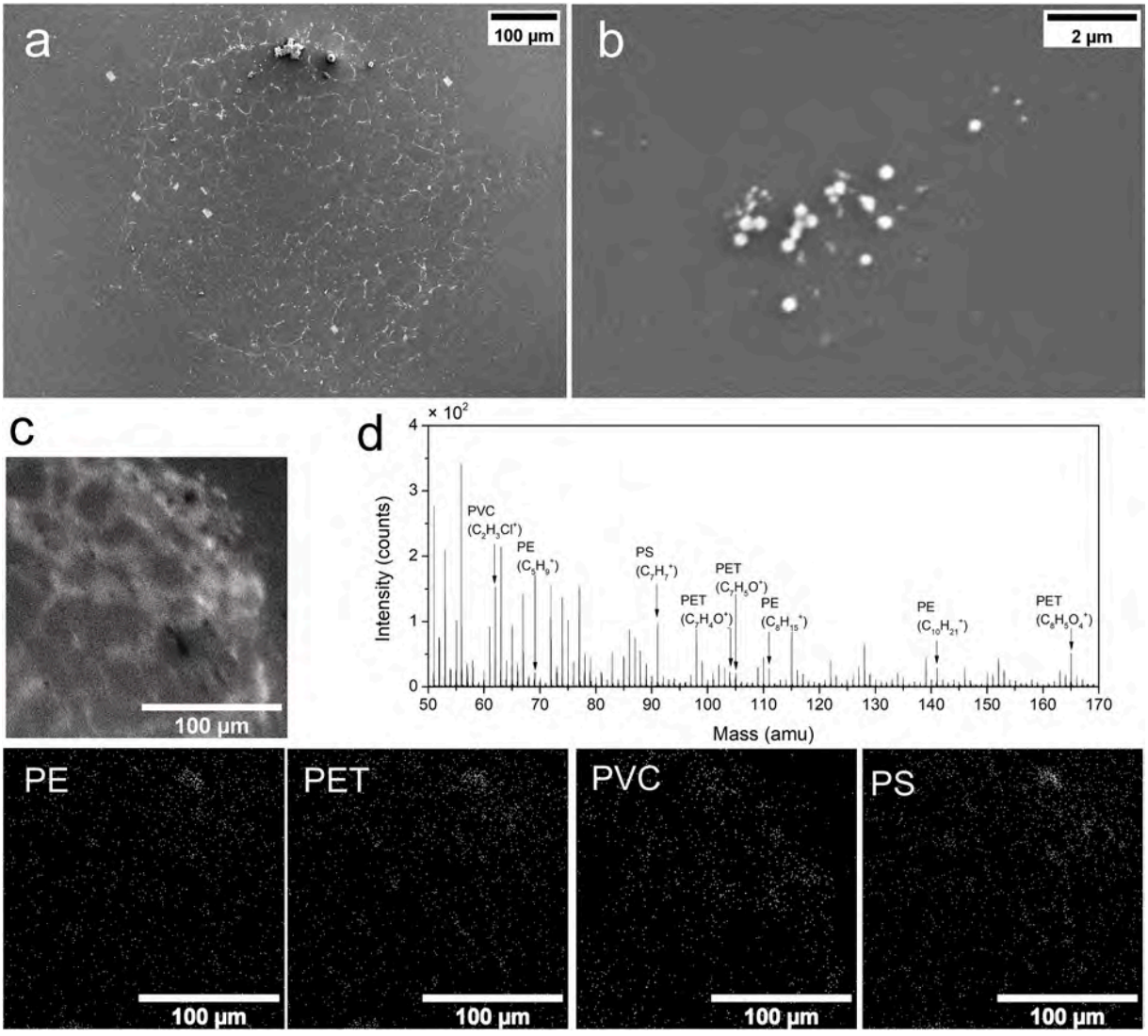

Fig. 4. SEM and ToF-SIMS images of mixtures of the four (polyvinyl chloride (PVC), polyethylene terephthalate (PET), polyethylene (PE), and polystyrene (PS)) submicron particles. (a) Full droplet and (b) partially magnified area of SEM images (c) ToF-SIMS total ion and specific plastic images and (d) mass spectrum. Specific plastic images were obtained by overlaying the representative m/z values of each plastic, and the detected pixel numbers of ion imaging were counted using ImageJ software.

3.4. Application for detecting submicron plastics released from hot water-treated teabags

3.4.1. Composition of teabags

Infrared spectra of teabags are shown in Fig. S8. The original teabag without tea leaves had characteristic peaks of PET and PE (Fig. S8a) (Jung et al., 2018). The other two original teabags with tea leaves exhibited peaks of PLA (Choksi and Desai, 2017) (Fig. S8b) and PET (Fig. S8c) (Jung et al., 2018).

3.4.2. Comparison of sizes and number concentrations using SEM and the NTA

Particle sizes and number concentrations of teabag leachates were measured by both SEM and the NTA. Fig. 5 and Table S2 respectively show SEM images and particle size distributions of the three teabag leachates. The particles all had spherical or elliptical shapes, with size distributions of 100–300 nm. Average particle sizes were 188 nm for PET/PE, 193 nm for PLA, and 181 nm for PET teabag leachates. Hydrodynamic sizes measured by the NTA were 156, 173, and 165 nm respectively.

The SEM-derived number concentrations were $2.45 \pm 0.03 \times 10^9$ (PET/PE), $2.93 \pm 0.27 \times 10^9$ (PLA), and $6.40 \pm 0.59 \times 10^8$ (PET) particles/mL. Relative errors between SEM-derived and NTA-derived concentrations were +8% ± 2% (PET/PE), +37% ± 13% (PLA), and +16% ± 18% (PET) (Table S3). The NTA-derived particle number concentration was $3.48 \pm 0.57 \times 10^7$ particles/mL for the blank experiment, which was 16–65-times lower than the teabag groups (Fig. 5). These results indicated that particle sizes and number concentrations obtained by SEM were more or less similar to those obtained by the NTA.

To compare the submicron plastic release capability among the three kinds of teabags, the particle number per unit area of a teabag (particles/cm^2) was expressed. The PLA teabag released the highest particle number per cm^2, followed by the PET/PE and PE teabags (Table S3). PLA has poor heat resistance, and it is more easily subjected to hydrolytic degradation compared to PET and PE (Rodriguez et al., 2016), which might explain these findings. Compared to results from Hernandez et al. (2019), our PET teabag released 3.67×10^9 particles/bag, which was lower than those of two teabags of the same composition (1.91×10^{10} and 2.14×10^{10} submicron particles/bag) (Table S3). The difference might be attributed to different teabag sizes or hot-water immersion times.

3.4.3. Confirmation of the composition by ToF-SIMS

Ion images of each type of plastic were made by overlaying their representative characteristic ions, and in this way, the location of the plastic particles was identified. PE and PET were characterized by the same mass-to-charge ratios as the method validation experiment. PLA was characterized by an m/z of 56.04 ($C_3H_4O^+$) (Manna et al., 2014).

Total ions and specific plastic ion images of teabag leachate are shown in Fig. 5. Original mass spectra are shown in Fig. S9. In the ion image of the PET/PE teabag leachate, respective pixel numbers of PET and PE at 200 × 200 μm^2 were 1932 and 1943. The ratio of pixel numbers (0.99) can be regarded as the number ratio of PET/PE particles due to their narrow size distribution as observed by SEM or the NTA. In ToF-SIMS images of PLA and PET teabag leachates, the specific plastic images corresponded well with the total ion results, which precisely confirmed the compositions of the particles. The compositions of the teabag leachates were qualitatively characterized by FTIR and x-ray photoelectron spectroscopy (Hernandez et al., 2019). As shown in this study, ToF-SIMS not only provided precise composition information, but also was able to determine the number ratio of different submicron plastics.

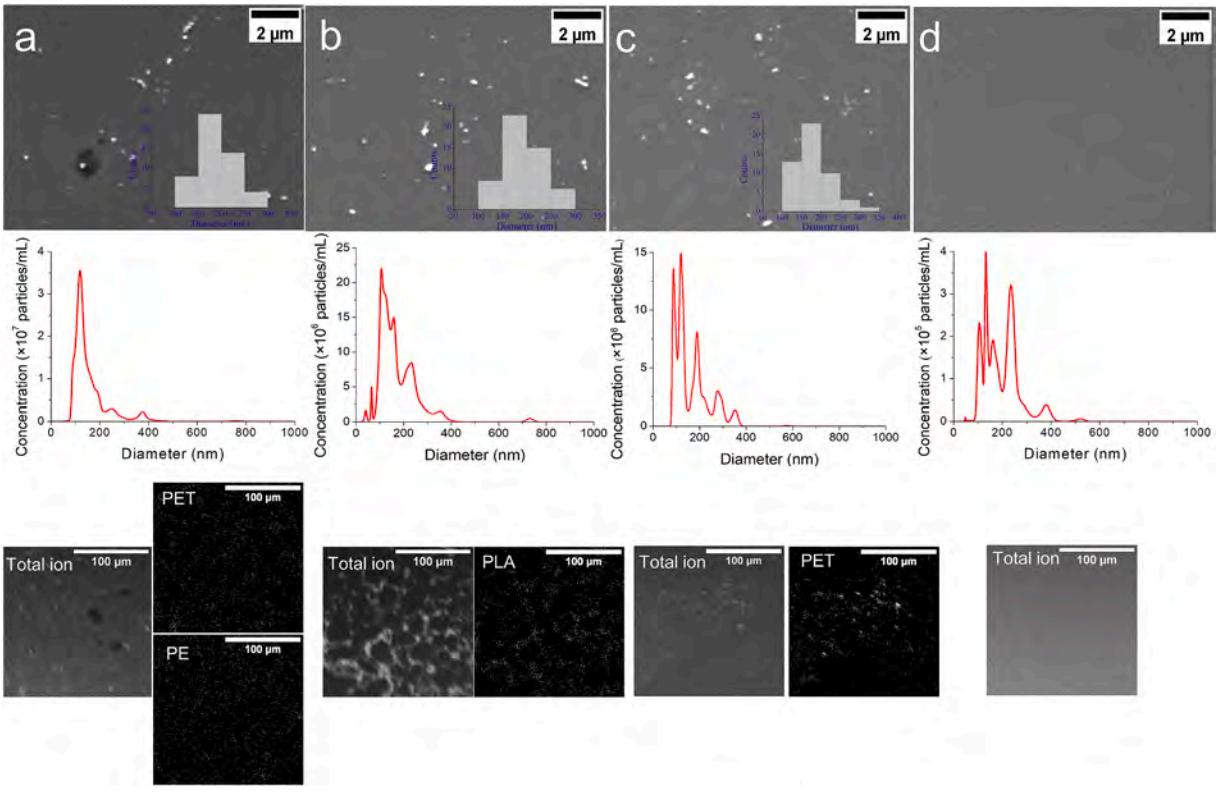

Fig. 5. SEM images, nanoparticle tracking analysis (NTA) size distributions, and ToF-SIMS images of submicron plastics released from hot-water-treated (a) polyethylene terephthalate (PET)/polyethylene (PE), (b) polylactic acid (PLA), and (c) PET teabags and the method blank (d). Particle sizes analyzed by SEM were 188 ± 40 (PET/PE), 193 ± 42 (PLA), and 181 ± 44 nm (PET) ($n = 50$) and hydrodynamic diameters measured via NTA were 156 ± 77 (PET/PE), 173 ± 85 (PLA), and 165 ± 75 nm (PET). The NTA-derived number concentration in the blank solution (without teabags) was $3.48 \pm 0.57 \times 10^7$ particles/mL, which was 16–65-times lower those of the teabag-containing groups.

3.5. NTA and SEM analyses after removing oligomers from the leachate

According to Busse et al.'s (2020) comments on a study by Hernandez et al. (2019), hydrosoluble oligomers released from PET teabags (37–214 μg/L) might crystallize when leachates are dried for the SEM analysis, and thus the particle number might be overestimated. To determine whether this assumption is correct, we used centrifugal concentrators with a 100-kDa membrane (with an estimated pore size of 10 nm) to separate particles and oligomers. All low-molecular-weight hydrosoluble oligomers of PET dimers to heptamers should be able to pass through the membrane, as was found in Tscochatzis et al.'s (2020) study of PET teabags. After analysis of the upper (which should have fewer oligomers) and bottom solutions (which should contain oligomers) by LC-MS, fewer of the PET or PLA oligomer types and lower abundances were identified in the upper solution than the bottom one, indicating that pretreatment effectively eliminated oligomers from the three teabag leachates (Table S4) (Tsochatzis et al., 2020; Ubeda et al., 2019). Interestingly, by comparing the NTA- and SEM-derived particle number concentrations of oligomers-contained with the deletion suspension, similar particle numbers were found in all leachates (Table S5, Fig. S10). Therefore, the particle number as determined by SEM was not overestimated because of the presence of oligomers. Interpretation of the slightly higher number detected by SEM than by NTA was not due to the presence of oligomers and requires further study.

3.6. Benefits and limitations of the method

Several studies have used SEM to quantify or visualize micro- or submicron-sized plastics released from hot-water-immersed plastic-containing food contact materials, such as teabags, infant feeding bottles (Li et al., 2020), and disposable paper cups (Ranjan et al., 2021), or from a face mask (Ma et al., 2021). However, details and limitations of the drop-casting procedures were not discussed. In this study, we clarified that the cleaning of the silicon wafer and dry-ice incubation before freeze-drying are important to suppress the coffee-ring effect. Submicron PS (0.195–1.040 μm), PET (0.311 μm), and PE (0.344 μm) could be effectively quantified. Although a concentration of at least 2.49×10^9 particles/mL should be prepared, only 20 nL (4.98×10^4 particles) was required for analysis. A combination of ToF-SIMS ion images could semi-quantitatively identify different submicron plastics, but the particles should have similar sizes. Due to limits of the quantitative analysis using ToF-SIMS, our developed method is more suitable for high-purity submicron-plastic samples, while it is not applicable to more-complex environmental samples containing non-plastic particles. It was noted that the common food contact material, PP, which was not addressed in this study, is hard to differentiate from PE by ToF-SIMS due to their similar mass spectra. Normalization of some positive ion peak intensities (e.g., $C_3H_5^+$) to $C_2H_3^+$ or negative ion peak intensity (C_6H^-) to C_4H^- can be a solution, but further studies are needed (Abmayr, 2006; Nie, 2016).

4. Conclusions

In this study, we successfully suppressed the coffee-ring effect by drop-casting submicron plastics using a silicon wafer cleaned with Piranha solution and dry-ice incubation before dripping, followed by freeze-drying. SEM images can be used to analyze the particle size, morphology, and number. Positive ion ToF-SIMS images can be used to qualitatively and semi-quantitatively identify submicron plastics. The developed method was then applied to analyze plastics released from teabags. Comparable size and particle number results were found between the SEM and NTA methods. The SEM analysis did not overestimate particle numbers due to the presence of oligomers. Estimation of the number ratio of PET and PE particles in teabag leachate by ToF-SIMS can provide more-informative data when the composition of food contact materials is complex.

Author statement

Shih-Hsuan Chou: Writing first draft of manuscript, conducting the SEM and ToF-SIMS experiments, synthesizing and characterizing the PE particles. **Yung-Kun Chuang**: Designing and conducting pre-treatment and analysis of oligomers. **Chi-Ming Lee:** ToF-SIMS measurement. **Yu-Shan Chang**: Synthesizing and characterizing the PVC particles. **Ya-Jhu Jhang**: Synthesizing and characterizing PET particles. **Ching-Wen Yeh:** Conducting LC-MS experiments. **Tai-Sing Wu**: Writing and explaining phenomenon. **Chun-Yu Chuang and I-Lun Hsiao:** Conceptualization, methodology, writing, editing. All authors are involved in reviewing and discussing of the manuscript.

Declaration of competing interest

The authors declare that they have no known competing financial interests or personal relationships that could have appeared to influence the work reported in this paper.

Acknowledgments

This work was supported by the Ministry of Science and Technology (MOST), Taiwan (107-2218-E-038-006-MY3) and Taipei Medical University (TMU), Taiwan (TMU106-AE1-B27 and 108-3805-011-111).

Appendix A. Supplementary data

Supplementary data to this article can be found online at https://doi.org/10.1016/j.envpol.2022.118964.

References

Abmayr, D.W., 2006. Polyolefin homopolymer and copolymer spectra by ToF-SIMS. Surf. Sci. Spectra 13, 117. https://doi.org/10.1116/11.20030803.

Anyfantakis, M., Geng, Z., Morel, M., Rudiuk, S., Baigl, D., 2015. Modulation of the coffee-ring effect in particle/surfactant mixtures: the importance of particle-interface interactions. Langmuir 31, 4113–4120. https://doi.org/10.1021/acs.langmuir.5b00453.

Bennet, F., Müller, A., Radnik, J., Hachenberger, Y., Jungnickel, H., Laux, P., Luch, A., Tentschert, J., 2020. Preparation of nanoparticles for ToF-SIMS and XPS analysis. JoVE 163, e61758. https://doi.org/10.3791/61758.

Busse, K., Ebner, I., Humpf, H.U., Ivleva, N., Kaeppler, A., Oßmann, B.E., Schymanski, D., 2020. Comment on "Plastic teabags release billions of microparticles and nanoparticles into tea. Environ. Sci. Technol. 54, 14134–14135. https://doi.org/10.1021/acs.est.0c03182.

Choksi, N., Desai, H., 2017. Synthesis of biodegradable polylactic acid polymer by using lactic acid monomer. Int. J. Appl. Chem. 13, 377–384.

Dümichen, E., Eisentraut, P., Bannick, C.G., Barthel, A.K., Senz, R., Braun, U., 2017. Fast identification of microplastics in complex environmental samples by a thermal degradation method. Chemosphere 174, 572–584. https://doi.org/10.1016/j.chemosphere.2017.02.010.

Fang, C., Sobhani, Z., Zhang, X., Gibson, C.T., Tang, Y., Naidu, R., 2020. Identification and visualisation of microplastics/nanoplastics by Raman imaging (ii): smaller than the diffraction limit of laser? Water Res. 183, 116046. https://doi.org/10.1016/j.watres.2020.116046.

Fang, C., Sobhani, Z., Zhang, X., McCourt, L., Routley, B., Gibson, C.T., Naidu, R., 2021. Identification and visualisation of microplastics/nanoplastics by Raman imaging (iii): algorithm to cross-check multi-images. Water Res. 194, 116913. https://doi.org/10.1016/j.watres.2021.116913.

Franssila, S., 2010. Introduction to Microfabrication, pp. 143–152. https://doi.org/10.1002/9781119990413.

Gigault, J., ElHadri, H., Nguyen, B., Grassl, B., Rowenczyk, L., Tufenkji, N., Feng, S., Wiesner, M., 2021. Nanoplastics are neither microplastics nor engineered nanoparticles. Nat. Nanotechnol. 16, 501–507. https://doi.org/10.1038/s41565-021-00886-4.

Gillibert, R., Balakrishnan, G., Deshoules, Q., Tardivel, M., Magazzù, A., Donato, M.G., Maragò, O.M., Lamy De La Chapelle, M., Colas, F., Lagarde, F., Gucciardi, P.G., 2019. Raman tweezers for small microplastics and nanoplastics identification in seawater. Environ. Sci. Technol. 53, 9003–9013. https://doi.org/10.1021/acs.est.9b03105.

He, E., Guo, D., Li, Z., 2019. A widely applicable strategy for coffee-ring effect suppression and controllable deposition of nanoparticles utilizing ice drying. Adv. Mater. Interfac. 6, 1900446. https://doi.org/10.1002/admi.201900446.

Hernandez, L.M., Xu, E.G., Larsson, H.C.E., Tahara, R., Maisuria, V.B., Tufenkji, N., 2019. Plastic teabags release billions of microparticles and nanoparticles into tea. Environ. Sci. Technol. 53, 12300–12310. https://doi.org/10.1021/acs.est.9b02540.

Hernandez, L.M., Yousefi, N., Tufenkji, N., 2017. Are there nanoplastics in your personal care products? Environ. Sci. Technol. Lett. 4, 280–285. https://doi.org/10.1021/acs.estlett.7b00187.

Holzlechner, G., Kubicek, M., Hutter, H., Fleig, J., 2013. A novel ToF-SIMS operation mode for improved accuracy and lateral resolution of oxygen isotope measurements on oxides. J. Anal. At. Spectrom. 28, 1080. https://doi.org/10.1039/c3ja50059d.

Jung, M.R., Horgen, F.D., Orski, S.V., Rodriguez, C.V., Beers, K.L., Balazs, G.H., Jones, T. T., Work, T.M., Brignac, K.C., Royer, S.J., Hyrenbach, K.D., Jensen, B.A., Lynch, J. M., 2018. Validation of ATR FT-IR to identify polymers of plastic marine debris, including those ingested by marine organisms. Mar. Pollut. Bull. 127, 704–716. https://doi.org/10.1016/j.marpolbul.2017.12.061.

Jungnickel, H., Pund, R., Tentschert, J., Reichardt, P., Laux, P., Harbach, H., Luch, A., 2016. Time-of-flight secondary ion mass spectrometry (ToF-SIMS)-based analysis and imaging of polyethylene microplastics formation during sea surf simulation. Sci. Total Environ. 563 (564), 261–266. https://doi.org/10.1016/j.scitotenv.2016.04.025.

Kern, S., Kern, C., Rohnke, M., 2019. Mass spectra database of polymers for bismuth-cluster ToF-SIMS. Surf. Sci. Spectra 26, 025003. https://doi.org/10.1116/1.5096485.

Li, D., Shi, Y., Yang, L., Xiao, L., Kehoe, D.K., Gun'ko, Y.K., Boland, J.J., Wang, J.J., 2020. Microplastic release from the degradation of polypropylene feeding bottles during infant formula preparation. Nat. Food. 1, 746–754. https://doi.org/10.1038/s43016-020-00171-y.

Lin, Y., Huang, X., Liu, Q., Lin, Z., Jiang, G., 2020. Thermal fragmentation enhanced identification and quantification of polystyrene micro/nanoplastics in complex media. Talanta 208, 120478. https://doi.org/10.1016/j.talanta.2019.120478.

Ma, J., Chen, F., Xu, H., Jiang, H., Liu, J., Li, P., Chen, C.C., Pan, Ke, 2021. Face masks as a source of nanoplastics and microplastics in the environment: quantification, characterization, and potential for bioaccumulation. Environ. Pollut. 288, 117748. https://doi.org/10.1016/j.envpol.2021.117748.

Manna, S., Augsburger, J.J., Correa, Z.M., Landero, J.A., Banerjee, R.K., 2014. Development of chitosan and polylactic acid based methotrexate intravitreal micro-implants to treat primary intraocular lymphoma: an in vitro study. J. Biomech. Eng. 136, 021018 https://doi.org/10.1115/1.4026176.

Materić, D., Kasper-Giebl, A., Kau, D., Anten, M., Greilinger, M., Ludewig, E., VanSebille, E., Röckmann, T., Holzinger, R., 2020. Micro-and nanoplastics in alpine snow: a new method for chemical identification and (semi)quantification in the nanogram range. Environ. Sci. Technol. 54, 2353–2359. https://doi.org/10.1021/acs.est.9b07540.

Mintenig, S.M., Bäuerlein, P.S., Koelmans, A.A., Dekker, S.C., VanWezel, A.P., 2018. Closing the gap between small and smaller: towards a framework to analyse nano- and microplastics in aqueous environmental samples. Environ. Sci. Nano 5, 1640–1649. https://doi.org/10.1039/c8en00186c.

Mitrano, D.M., Wick, P., Nowack, B., 2021. Placing nanoplastics in the context of global plastic pollution. Nat. Nanotechnol. 16, 491–500. https://doi.org/10.1038/s41565-021-00888-2.

Molenaar, R., Chatterjee, S., Kamphuis, B., Segers-Nolten, I.M.J., Claessens, M.M.A.E., Blum, C., 2021. Nanoplastic sizes and numbers: quantification by single particle tracking. Environ. Sci. Nano 8, 723–730. https://doi.org/10.1039/D0EN00951B.

Nie, H.Y., 2016. Negative hydrocarbon species $C_{2n}H^-$: how useful can they be? J. Vac. Sci. Technol. B 34, 030603. https://doi.org/10.1116/1.4941725.

Rangarajan, S., Tyler, B.J., 2006. Topography in secondary ion mass spectroscopy images. J. Vac. Sci. Technol. 24, 1730. https://doi.org/10.1116/1.2217980.

Ranjan, V.P., Joseph, A., Goel, S., 2021. Microplastics and other harmful substances released from disposable paper cups into hot water. J. Hazard Mater. 404, 124118. https://doi.org/10.1016/j.jhazmat.2020.124118.

Rodriguez, E.J., Marcos, B., Huneault, M.A., 2016. Hydrolysis of polylactide in aqueous media. J. Appl. Polym. Sci. 133, 44152. https://doi.org/10.1002/app.44152.

Schwaferts, C., Sogne, V., Welz, R., Meier, F., Klein, T., Niessner, R., Elsner, M., Ivleva, N. P., 2020. Nanoplastic analysis by online coupling of Raman microscopy and field-flow fractionation enabled by optical tweezers. Anal. Chem. 92, 5813–5820. https://doi.org/10.1021/acs.analchem.9b05336.

Shishido, R., Fujii, M., Seki, T., Aoki, T., Matsuo, J., Suzuki, S., 2016. Yields and images of secondary ions from organic materials by different primary Bi ions in time-of-flight secondary ion mass spectrometry. Rapid Commun. Mass Spectrom. 30, 476–482. https://doi.org/10.1002/rcm.7455.

Sun, J., Bao, B., He, M., Zhou, H., Song, Y., 2015. Recent advances in controlling the depositing morphologies of inkjet droplets. ACS Appl. Mater. Interfaces 7, 28086–28099. https://doi.org/10.1021/acsami.5b07006.

TerHalle, A., Jeanneau, L., Martignac, M., Jardé, E., Pedrono, B., Brach, L., Gigault, J., 2017. Nanoplastic in the North Atlantic subtropical Gyre. Environ. Sci. Technol. 51, 13689–13697. https://doi.org/10.1021/acs.est.7b03667.

Tsochatzis, E.D., Alberto Lopes, J., Kappenstein, O., Tietz, T., Hoekstra, E.J., 2020. Quantification of PET cyclic and linear oligomers in teabags by a validated LC-MS method – in silico toxicity assessment and consumer's exposure. Food Chem. 317, 126427. https://doi.org/10.1016/j.foodchem.2020.126427.

Ubeda, S., Aznar, M., Alfaro, P., Nerín, C., 2019. Migration of oligomers from a food contact biopolymer based on polylactic acid (PLA) and polyester. Anal. Bioanal. Chem. 411, 3521–3532. https://doi.org/10.1007/S00216-019-01831-0.

Zhang, W., Dong, Z., Zhu, L., Hou, Y., Qiu, Y., 2020. Direct observation of the release of nanoplastics from commercially recycled plastics with correlative Raman imaging and scanning electron microscopy. ACS Nano 14, 7920–7926. https://doi.org/10.1021/acsnano.0c02878.

Zhou, X.X., Hao, L.T., Wang, H.Y.Z., Li, Y.J., Liu, J.F., 2019. Cloud-point extraction combined with thermal degradation for nanoplastic analysis using pyrolysis gas chromatography-mass spectrometry. Anal. Chem. 91, 1785–1790. https://doi.org/10.1021/acs.analchem.8b04729.